Am J Physiol Heart Circ Physiol 320: H1276–H1289, 2021.
First published January 29, 2021; doi:10.1152/ajpheart.00571.2020

american physiological society

AMERICAN JOURNAL OF PHYSIOLOGY
HEART AND CIRCULATORY PHYSIOLOGY

RESEARCH ARTICLE

Exosomes and Extracellular Vesicles in Cardiovascular Physiology

Characterization of βARKct engineered cellular extracellular vesicles and model specific cardioprotection

Jin-Sook Kwon,[1] Sarah M. Schumacher,[1] Erhe Gao, J. Kurt Chuprun,[1] Jessica Ibetti,[1] Rajika Roy,[1] Mohsin Khan,[2] Raj Kishore,[1] and Walter J. Koch[1]

[1]*Center for Translational Medicine, Department of Pharmacology, Lewis Katz School of Medicine, Temple University, Philadelphia, Pennsylvania; and* [2]*Center for Metabolic Disease Research, Lewis Katz School of Medicine, Temple University, Philadelphia, Pennsylvania*

Abstract

Recent data supporting any benefit of stem cell therapy for ischemic heart disease have suggested paracrine-based mechanisms via extracellular vesicles (EVs) including exosomes. We have previously engineered cardiac-derived progenitor cells (CDCs) to express a peptide inhibitor, βARKct, of G protein-coupled receptor kinase 2, leading to improvements in cell proliferation, survival, and metabolism. In this study, we tested whether βARKct-CDC EVs would be efficacious when applied to stressed myocytes in vitro and in vivo. When isolated EVs from βARKct-CDCs and control GFP-CDCs were added to cardiomyocytes in culture, they both protected against hypoxia-induced apoptosis. We tested whether these EVs could protect the mouse heart in vivo, following exposure either to myocardial infarction (MI) or acute catecholamine toxicity. Both types of EVs significantly protected against ischemic injury and improved cardiac function after MI compared with mice treated with EVs from mouse embryonic fibroblasts; however, βARKct EVs treated mice did display some unique beneficial properties including significantly altered pro- and anti-inflammatory cytokines. Importantly, in a catecholamine toxicity model of heart failure (HF), myocardial injections of βARKct-containing EVs were superior at preventing HF compared with control EVs, and this catecholamine toxicity protection was recapitulated in vitro. Therefore, introduction of the βARKct into cellular EVs can have improved reparative properties in the heart especially against catecholamine damage, which is significant as sympathetic nervous system activity is increased in HF.

NEW & NOTEWORTHY βARKct, the peptide inhibitor of GRK2, improves survival and metabolic functions of cardiac-derived progenitor cells. As any benefit of stem cells in the ischemic and injured heart suggests paracrine mechanisms via secreted EVs, we investigated whether CDC-βARKct engineered EVs would show any benefit over control CDC-EVs. Compared with control EVs, βARKct-containing EVs displayed some unique beneficial properties that may be due to altered pro- and anti-inflammatory cytokines within the vesicles.

βARKct; cardiac derived cells; cardiomyocytes; extracellular vesicles; GRK2; microRNAs

INTRODUCTION

Myocardial infarction (MI) is a leading cause of mortality and morbidity in developed nations, and there remains a need for effective therapies that significantly mitigate tissue damage or regenerate the myocardium. Embryonic stem cells, adult stem cells, and progenitor cell types have been attractive candidates for treatment for post-MI heart failure (HF), however, these cells have not led to any significant therapies as of yet and controversy remains that they will never be effective (1). Accordingly, next-generation cell-based therapies have been emerging and much attention has now shifted to secreted vesicles from various stem and progenitor cell populations (2–4). This research began since injected stem cells do not remain in the heart and do not differentiate into adult myocytes, but potential benefits suggest a paracrine mechanism from the cells (5) or substances released from dying cells (6). Thus, attention has turned to delivering purified exosomes secreted from various stem/progenitor cells.

Exosomes are secreted extracellular vesicles with a cell-manufactured lipid bilayer and range in size from 50 nm to 150 nm in diameter (7). They can be isolated from numerous cell lines (8) and also body fluids, including saliva, blood, pericardial fluid, and urine (9). Typically, exosomes carry nucleic acids and proteins, and critical cargo include

Correspondence: W. J. Koch (walter.koch@temple.edu).
Submitted 23 July 2020 / Revised 20 January 2021 / Accepted 20 January 2021

noncoding RNAs such as micro-RNAs (10, 11). Studies have shown that the environment that cells are grown in or are exposed to can alter the characteristics of exosome cargo, however, the specificity of such changes is still not fully understood (8, 12). Accordingly, in fields such as cancer, exosomes from patient blood are being explored as biomarkers for both disease and treatment response (13). Moreover, there has been research into using exosomes as specific carriers for gene therapy or small molecule therapeutics (14, 15). Importantly, exosome delivery as antitumor therapy in humans was found to be safe (16).

As aforementioned, in the cardiovascular field, attention has turned from stem/progenitor cell injections after MI to exosomes. In particular, stem/progenitor cell-derived exosomes have been used to rescue post-MI HF in animal models (2–4). A few studies used exosomes purified from a resident c-kit$^+$ cardiac-derived progenitor cell (CDC) (17–19), a cell that has been the center of controversy in the cardiovascular arena (20, 21). Regardless of the true nature of these CDCs, exosomes from these cells, when injected into the post-MI heart, enhance endothelial cell migration, indicating angiogenic effects and also have been shown to reduce myoblast apoptosis in vitro (19) and decrease myocyte cell death post-MI (17). Interestingly, exosomes from CDCs exposed to hypoxia had improved reparative properties in vivo when compared with exosomes isolated from normoxic cells (18).

The latter observation raises the notion that the myocardial reparative properties of exosomes, especially from this CDC population, could be enhanced either via the environment or altered signaling pathways within cells. On this note, we have previously engineered CDCs to express a peptide inhibitor of G protein-coupled receptor kinase 2 (GRK2), which led to improved metabolic properties of these cells and also enhanced proliferation and survival after stress compared with control CDCs expressing green fluorescent protein (GFP) (22) This peptide, βARKct, inhibits the G protein activation of GRK2 as well as its mitochondrial-localized cell death activity (23). Myocardial βARKct expression has been shown to protect against ischemic injury and death and also reverse post-MI HF (24–26). Therefore, we hypothesize that extracellular vesicles (EVs) including exosomes (hereafter referred to as EVs) from cells expressing βARKct may have enhanced reparative properties for the injured myocardium. Accordingly, in this study, we have characterized EVs from βARKct-containing CDCs, comparing them to EVs from control GFP-CDCs. We have tested their prosurvival properties in myocytes after hypoxia- or catecholamine-induced injury in vitro as well as their in vivo reparative properties against injured and stressed myocardium in the mouse.

METHODS

Extracellular Vesicle Generation from CDCs

Mouse cardiac-derived c-Kit$^+$ cells (CDCs) previously modified to stably express the βARKct peptide (βARKct-CDCs) or GFP-CDCs were cultured as described (22). CDCs containing βARKct also contained GFP as the lentivirus used had a bicistronic cassette for this marker protein (22). Cells from passage 21 to 27 were used to generate extracellular vesicles (EVs). CDCs were cultured to 90% confluence in DMEM: F12 (1:1) media with 10% fetal bovine serum (FBS), Insulin-Transferrin-Selenium (ITS, Lonza, 17-838Z), fibroblast growth factor (FGF, Peprotech, AT-100-18B), epidermal growth factor (EGF, Peprotech, AT-100-15), leukemia inhibitory factor (LIF, Millipore, ESG-1107), and 1% penicillin-streptomycin (PS), and then at 90% confluence the media was changed to DMEM: F12 (1:1) without FBS but containing ITS, FGF, EGF, LIF, and PS. We have used the differential ultracentrifugation method, the method used to isolate exosomes over the past few years, to isolate EVs. After 40 h, the cell media were collected and subjected to sequential centrifugation at 4,400 rpm for 15 min (Centrifuge 5702 R, Eppendorf) and then at 10,000 *g* for 30 min to remove cell debris, and finally at 100,000 *g* for 75 min (Optima L-90K ultracentrifuge, Beckman Coulter SW 70 Ti rotor). The EVs were washed once in PBS and collected by centrifugation at 100,000 *g* for 60 min. The EVs pellet was resuspended in PBS and an aliquot was used to measure EVs number and size distribution using Nanosight technology (model NS300, Malvern Instruments Ltd., Worcestershire, UK) according to the manufacturer's instructions (27). Remaining EVs were stored at −70°C until further use. The primary mouse embryonic fibroblast (MEF) cell line was purchased form Sigma-Aldrich (untreated PMEF, passage 3). The MEF were cultured up to 5 passages in DMEM with 10% FBS, 1% PS, and 1% L-glutamine and then changed to DMEM with 10% exosome free FBS (EF-FBS) and PS. After 40 h, the cell media were collected and EVs were isolated by differential ultracentrifugation.

Western blotting for the exosomal marker proteins, flotillin, and HSP70 was also performed.

To examine EVs morphology, electron microscopy was performed on a Joel 1010 transmission electron microscope (Joel Ltd, Warwickshire, UK) after a standard staining procedure with 0.5% uranyl acetate.

Gene Chip miRNA Array

EVs were isolated and total RNA was prepared using the miRNeasy kit (Qiagen) according to the manufacturer's instructions. Gene chip miRNA array was conducted by Fox Chase Cancer Center, Genomics Facility. Total RNA concentration was measured using the 2100 Bioanalyzer with Eukaryote Total RNA nano (Affymetrix). The microarray assay was performed using the GeneChip miRNA 4.0 assay protocol from Thermo Fisher Scientific. For each sample, 130 ng of RNA was labeled using the FlashTag Biotin RNA Labeling Kit (Thermo Fisher Scientific). The labeled RNA was quantified, fractionated, and hybridized to the miRNA 4.0 microarray according to the manufacturer's instructions. The miRNA microarray chips were washed and stained using the Genechip Fluidics Station 450. Finally, the miRNA microarray chips were scanned using an Affymetrix GCS 3000 scanner, and the signal values were evaluated using the Affymetrix GeneChip Command Console software.

RNA Extraction/cDNA Synthesis/Reverse Transcriptase-Quantitative Polymerase Chain Reaction for miRNA Expression

EVs were isolated and total RNA was prepared using the miRNeasy kit (Qiagen) according to the manufacturer's instructions. Total RNA concentration was measured using

the NanoDrop 2000 (Thermo Fisher Scientific). cDNA was synthesized using the miRScript II RT kit (Qiagen). cDNA was subjected to reverse transcriptase-quantitative polymerase chain reaction (RT-qPCR) using iQ SYBR Green Supermix (Bio-Rad) on the CFX96 Touch System (Bio-Rad), using the thermal profile suggested by the manufacturer. Expression levels of miRNAs in the GFP and βARKct EVs were quantitatively compared using the ΔΔCt method with 5S-rRNA as the endogenous control for expression.

The following miRCURY LNA miRNA primers for miRNA expression were purchased from Exiqon: mmu-mir-346-5p, mmu-miR-7004-5p, mmu-miR-3065-5p, mmu-miR-7b-3p, mmu-miR-1903, mmu-miR-3473f, and *5S*.

The following miScript Primer Assays were purchased from Qiagen, *SNORD95* (MS00033733), *SNORD96A* (MS00033726), RNU6-2(MS00033740), mmu-mir-294-3p (MS00001988), and mmu-mir-294-5p (MS00032627).

In Supplemental Fig. S2 (all Supplemental Material available at https://doi.org/10.6084/m9.figshare.13604135.v1), the expression levels of mmu-miR-294 in the GFP, βARKct, and MEF EVs were quantitatively compared using the ΔΔCt method with *SNORD95*, *SNORD96A*, and *RNU6-2*, as the reference genes used for normalization.

Hypoxia and Combined Hypoxia with Isoproterenol in NRVMs to Simulate In Vivo Ischemic Injury

Neonatal rat ventricle cardiomyocytes (NRVMs) were isolated from neonatal rat ventricles (1- to 2-days-old), as previously described (28). The isolated cells were cultured in Ham's F10 Medium (Corning) supplemented with 10% horse serum (HS), 5% FBS, and 1% PS. The day after plating, NRVM were washed in phosphate-buffered saline (PBS) and were cultured in in Ham's F10 without FBS and 2×10^{10} EVs were added for 4 h. The cells were then placed into a hypoxia chamber (CO_2/O_2 incubator, Galaxy 14S, Eppendorf) with 1% O_2, 5% CO_2. To quantify the number of apoptotic cells after 20 h of hypoxia, TUNEL staining was performed according to the instructions of the In Situ Cell Death Detection Kit, Fluorescein (Roche). For immunoblotting and measurement of caspase 3 activity, NRVMs were harvested after 4 and 20 h. Hypoxia- and isoproterenol-combined injury were conducted by adding isoproterenol (Iso, 100 μM) in the media after 4 h of EVs pretreatment and then placed into the hypoxia chamber for 4 and 20 h. Caspase 3 activity was measured in these cells with the colorimetric Caspase 3 Assay kit (Abcam ab39401) according to the manufacturer's instructions.

Immunoblotting Assay and Immunohistochemistry

EVs, CDC, NRVMs, and mouse heart tissue total protein was extracted using ice-cold radioimmunoprecipitation assay (RIPA) buffer with protease and phosphatase inhibitor (Sigma-Aldrich), and protein concentration was measured by the BCA method (Pierce). For immunoblotting, protein samples were loaded on 4%–20% Tris-glycine precast gels (Bio-Rad) and transferred to nitrocellulose membrane. Primary antibodies were diluted in Odyssey blocking buffer (Li-Cor Biosciences) and incubations were performed overnight at 4°C. Primary antibodies were obtained from the following vendors: Flotillin and HSP70 (Abcam); GRK2 (to detect the βARKct), GFP, and GAPDH (Santa Cruz); Akt, p-Akt and Caspase 3 (Cell Signaling). Visualization of immunoblot signals was performed using secondary antibodies coupled to Alexa Fluor 680 (Invitrogen Molecular Probes) or IRDye 800 (LI-COR Biosciences) and imaged using the Odyssey CLx infrared imager (LI-COR Biosciences). Odyssey v. 1.2 imaging software was used to process the images.

Induction of Acute Myocardial Infarction

Male mice, C57BL/6 at 8 wk of age were purchased from The Jackson Laboratories (Bar Harbor, ME). All surgical procedures and animal care protocols were approved by the Temple University Animal Care and Use Committee. At 9 wk of age mice underwent MI surgery by ligating the left anterior descending (LAD) coronary artery as reported previously (29). Concurrently, 1×10^8 EVs from GFP-CDC, βARKct-CDC, or MEF cells were suspended in 5 μL of PBS and administered by intramyocardial injection into the anterior wall, posterior wall, and apex of the left ventricle. Total injection volume for each heart was 15 μL and contained $3 \times 10^8 \pm 7.5\%$ EVs. The PBS group underwent the same surgery but received PBS without EVs, and the sham group underwent surgery without ligation.

High Dose Isoproterenol Injury Model

The high dose isoproterenol (Iso) injury model was performed essentially as described with minor modification (30). EVs (3×10^8) were injected into the LV and 8 h later the first dose of Iso (300 mg/kg/day) was administered via dorsal subcutaneous (SQ) injection. Iso was administered daily for an additional 4 days (five total injections). A baseline echo was performed 2 days before EVs delivery, then again 1 and 2 wk after EVs delivery, at which time the study ended and the mice were euthanized and hearts obtained for histological analysis. A control group of mice received an LV injection of PBS instead of EVs, and PBS was administered via dorsal SQ instead of Iso.

Echocardiography

Echocardiography was performed using the Vevo 2100 imaging system from VisualSonics as described previously (31). Briefly, two-dimensional echocardiographic views of the midventricular short axis were obtained at the level of the papillary muscle tips below the mitral valve. M-mode measurements were determined at the plane bisecting the papillary muscles according to the American Society of Echocardiography's leading-edge method.

Tissue Preparation for Biological and Histological Analysis

Mice were anesthetized by isoflurane or avertin and blood was collected from the carotid artery. For biological analysis, hearts were washed using cold PBS immediately after collecting blood and stored at −80°C. Hearts for histologic analysis were harvested after cardioperfusion and fixed in 4% PFA at 4°C for 1–3 days with rocking. Hearts were dehydrated and paraffinized using the Microm STP 120 from Thermo Fisher Scientific, embedded in paraffin using a HistoStar apparatus (Thermo Fisher Scientific), and sectioned (6 μm) using the Microm HM 325 (Thermo Fisher Scientific). Tissue sections were stained with Weigert's iron hematoxylin and

Masson trichrome (Sigma-Aldrich) according to the manufacturer's instructions. Area and length of heart and MI region was measured using Nis-Element (v. 4.0) from at least three sections of one heart. For immunofluorescence staining, tissue sections were deparaffinized and rehydrated according to the trichrome staining protocol, but after the wash with deionized water, heart sections were washed three times for 5 min with PBS, followed by blocking using 10% BSA for 1 h and incubated with primary antibody overnight. The secondary antibody was conjugated to Alexa Fluor 488 or 594 (1:100 or 1:200 in PBS) for 1 h at room temperature in a humidified chamber in the dark. Tissue sections were again washed three times for 5 min with PBS, followed by mounting with coverslips using Fluoromount-G with DAPI mounting media (Southern Biotech). We used anti-α-sarcomeric actin antibody (Sigma, A7811) and anti-MPO antibody (Santa Cruz, SC-390109). Immunohistochemical staining was performed according to the manufacturer's instructions with minor modification using antigen unmasking solution (VECTOR), biotinylated anti-mouse (BA-2001), rabbit IgG (BA-1000) Ab, VECTASTAIN ABC kit and DAB (VECTOR, SK-4100). For terminal deoxynucleotidyl transferase-mediated deoxyuridine triphosphate nick end labeling (TUNEL) staining to identify apoptotic cardiomyocytes, heart sections were stained by α-sarcomeric actin without the antigen unmasking step and then TUNEL stain was performed according to instructions of In Situ Cell Death Detection Kit, Fluorescein (Roche).

Measurement of Cytokine and BNP Gene Expression in Heart Tissue

Total RNA isolations from heart were performed using the miRNEasy kit (Qiagen), and cDNA was synthesized using oligo-(dT) primer and reverse transcriptase (Bio-Rad) according to the manufacturer's protocol. Using the primer sequences shown below (Sigma Aldrich), synthesized cDNA samples were subjected to real time RT-qPCR (Bio-Rad CFX96 Touch) using iQ SYBR Green Supermix (Bio-Rad). Expression levels between the various groups were quantitatively compared using the ΔΔCt method with mouse glyceraldehyde-3-phosphate dehydrogenase (GAPDH) as the endogenous control for target gene expression.

The primers sequences (written 5′-3′) were: *IL-6*, forward: CCCCAATTTCCAATGCTCTCC, reverse: CGCACTAGGTTTGCCGAGTA; *IL-10*, forward: TAACTGCACCCACTTCCCAG, reverse: AGGCTTGGCAACCCAAGTAA; *MCP-1*, forward: CCCAATGAGTAGGCTGGAGA, reverse: TCTGGACCCATTCCTTCTTG; *CCL-4*, forward: CCCACTTCCTGCTGTTTCTC, reverse: GTCTGCCTCTTTTGGTCAGG; *BNP*, forward: CTGAAGGTGCTGTCCCAGAT, reverse: CCTTGGTCCTTCAAGAGCTG; *GAPDH*, forward: CCCTTAAGAGGGATGCTGCC, reverse: TACGGCCAAATCCGTTCACA.

Statistics

For experiments in mice, results are presented as means ± SE, and in cell experiments using NRVMs, results are represented as means ± SD, computed from the average measurement obtained from each three or four repeat experiments. Comparison of three or more groups is performed by one-way or two-way ANOVA with Tukey's multiple comparisons test or nonpaired *t* test. $P < 0.05$ is considered statistically significant. Statistical analysis was performed using Graph Pad prism v. 8.0 software.

RESULTS

β ARKct-CDC EVs Characterization and microRNA (miRNA) Content

Our previous studies focused on how the GRK2 inhibitory peptide, βARKct, altered the proliferative, metabolic, and overall survival properties of CDCs, and indeed, the presence of the βARKct did improve all of these conditions (22). In this study, we wanted to determine if EVs from these genetically engineered cells could transfer these beneficial properties to stressed myocytes and if the presence of this peptide alters content or cargo. We used multiple approaches to characterize and confirm the purity of the isolated EVs. First, the protein band pattern of the EVs was analyzed by Coomassie Blue staining of the gel, and we found it to be different than that of the original cellular lysate from which the EVs were isolated (Supplemental Fig. S1*A*). Next, the isolated vesicles were enriched in the protein markers HSP70 and flotillin which is characteristic of EVs (Supplemental Fig. S1*B*). Finally, we examined the morphology and size distribution and found that the vesicles were appropriately sized as determined by the electron microscopy and Nanosight. The mode size of GFP-CDC-EVs and βARKct-CDC EVs were similar (GFP-CDC EVs, 119.67 ± 6.66 nm, βARKct-CDC EVs, 116.47 ± 2.81 nm) (Supplemental Fig. S1, *C* and *D*).

Both GFP and βARKct were identified by immunoblot to be present in the exosomes (Supplemental Fig. S1*B*). Since previous studies have shown miRNAs to be a major component of exosomal cargo that can have beneficial properties on the injured heart (32), we first examined whether the miRNA content from βARKct-CDC EVs differed significantly from control GFP-CDC EVs. We isolated RNA from purified CDC EVs and carried out a miRNA array analysis. Shown in Fig. 1*A* is the comparison between miRNA content from βARKct-CDC EVs versus GFP-CDC EVs. Using a twofold threshold (P value < 0.05), we found limited differences in the miRNA content between the two sets of EVs, with only six miRNAs upregulated in the βARKct-CDC EVs and 10 species downregulated (Fig. 1*B*). Validation using quantitative RT-PCR using exosomal RNA content confirmed that of the six candidates that emerged from the array, two miRNAs were significantly upregulated with βARKct present in EVs, these being miRNA-7004 and miRNA-7b (Fig. 1*C*) (P value < 0.05).

In Vitro Delivery and Effects of β ARKct-CDC EVs on Cardiomyocyte Survival Signaling and Cell Death after Hypoxic Stress

A major goal of this study was to determine if EVs from βARKct-containing CDCs had beneficial protective properties on the ischemic heart and to explain any effects that have been seen when CDCs were injected into the ischemic heart as a paracrine mechanism. We initially examined survival signaling via the activation of the survival kinase Akt in NRVMs and found that both βARKct-CDC EVs (P value < 0.01) and GFP-CDC EVs (P value < 0.001), when

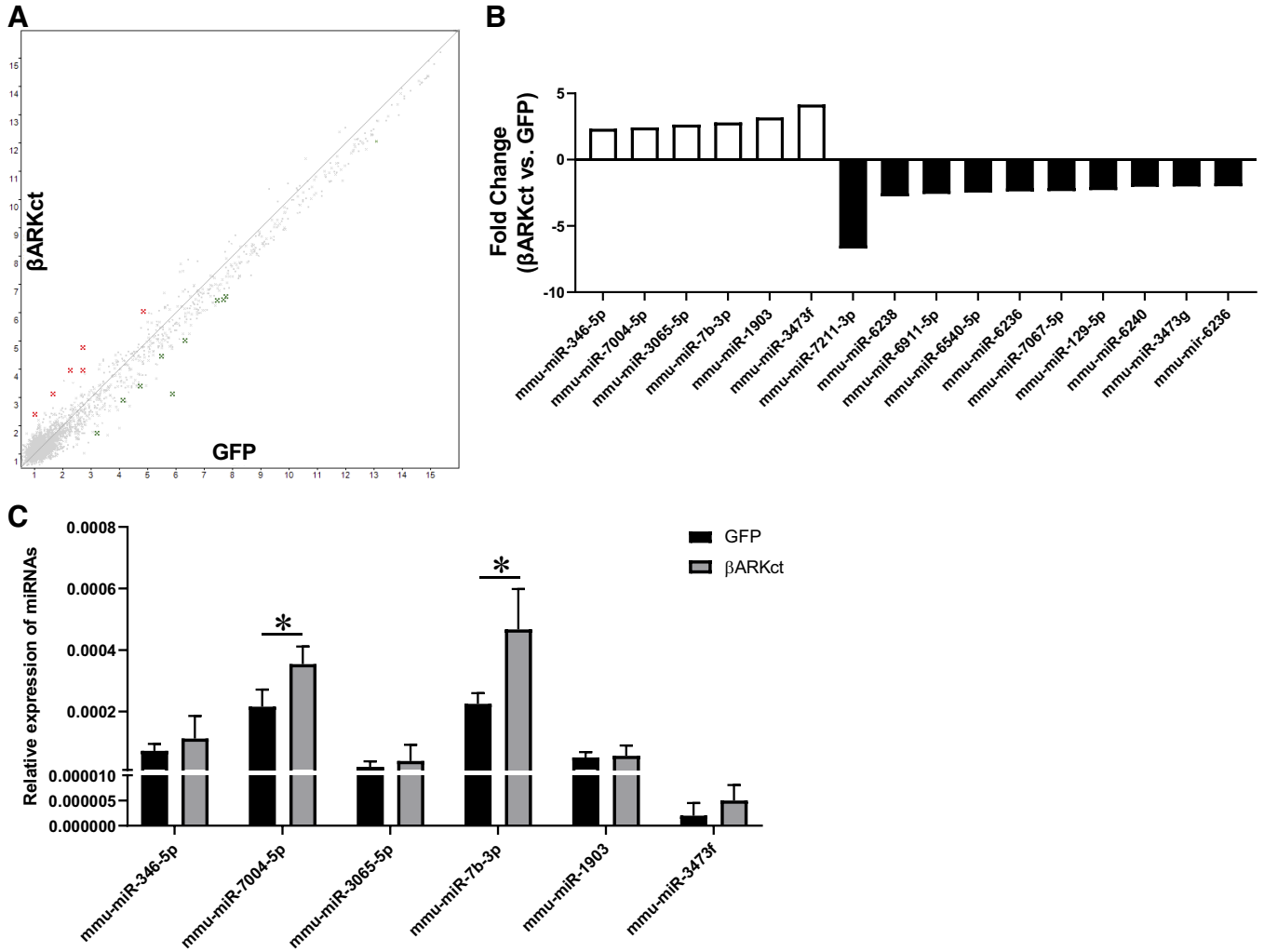

Figure 1. Analysis of miRNA expression profile of βARKct and green fluorescent protein (GFP) extracellular vesicle from cardiac-derived progenitor cells (CDC) using miRNA array. *A*: scatter plot of miRNA expression profiles. Selected upregulated miRNAs (red) and downregulated miRNAs (green) by βARKct transduction compared with GFP transduction. *B*: bar graph of fold change of upregulated and downregulated miRNAs from the GeneChip *miRNA* 4.0 Array ($n = 2$). *C*: bar graph of RT-qPCR of six upregulated miRNAs. Means ± SD, nonpaired *t* test, $^*P < 0.05$, $n = 3$.

added to NRVMs in culture, activated Akt significantly compared with vehicle-treated NRVMs and myocytes treated with EVs from mouse embryonic fibroblasts (MEFs) as negative controls that showed no Akt activation (Fig. 2, *A* and *B*). Next, we determined if activation of Akt was altered in NRVMs under hypoxic stress and whether EVs had any effect on the activation status of this survival kinase. As expected in vehicle-treated control conditions, 4 h of hypoxic stress caused a significant reduction of activated Akt compared with myocytes under normoxic conditions (P value < 0.001), whereas EVs treatment (using 2×10^{10} exosomes) before hypoxia resulted in attenuation of this decrease (Fig. 2, *C* and *D*). As with treatment of normal NRVMs, the improvement in Akt activation trended to be higher with βARKct-CDC EVs (GFP EVs; P value < 0.01 and βARKct EVs; $P < 0.005$). Importantly, the significant myocyte cell death induced by chronic hypoxia that was seen after vehicle treatment ($P < 0.001$), as measured by TUNEL staining, was significantly attenuated by both types of EVs with limited NRVM apoptosis even after 20 h of hypoxia (GFP EVs; P value < 0.005 and βARKct EVs; $P < 0.001$) (Fig. 2*E*). To gain mechanistic insight into the effects of CDC-derived EVs on myocyte cell death after hypoxia, we examined cleaved caspase 3 after 20 h of hypoxia and saw a significantly lower level of this proapoptotic marker with both type of CDC EVs compared with the higher cleaved caspase 3 in saline-treated control myocytes (GFP EVs; $P < 0.05$ and βARKct EVs; $P < 0.05$) (Fig. 2, *F* and *G*).

In Vivo Delivery and Effects of β ARKct-CDC and GFP-CDC EVs in a Mouse Model of Myocardial Infarction and Heart Failure

Previous studies have shown that prepared from CDCs after exposure to hypoxic culture conditions provided some therapeutic benefit when delivered to the ischemic mouse heart after MI (18). We wanted to test whether EVs from CDCs that were engineered to have better survival and metabolism via βARKct expression would offer any therapeutic

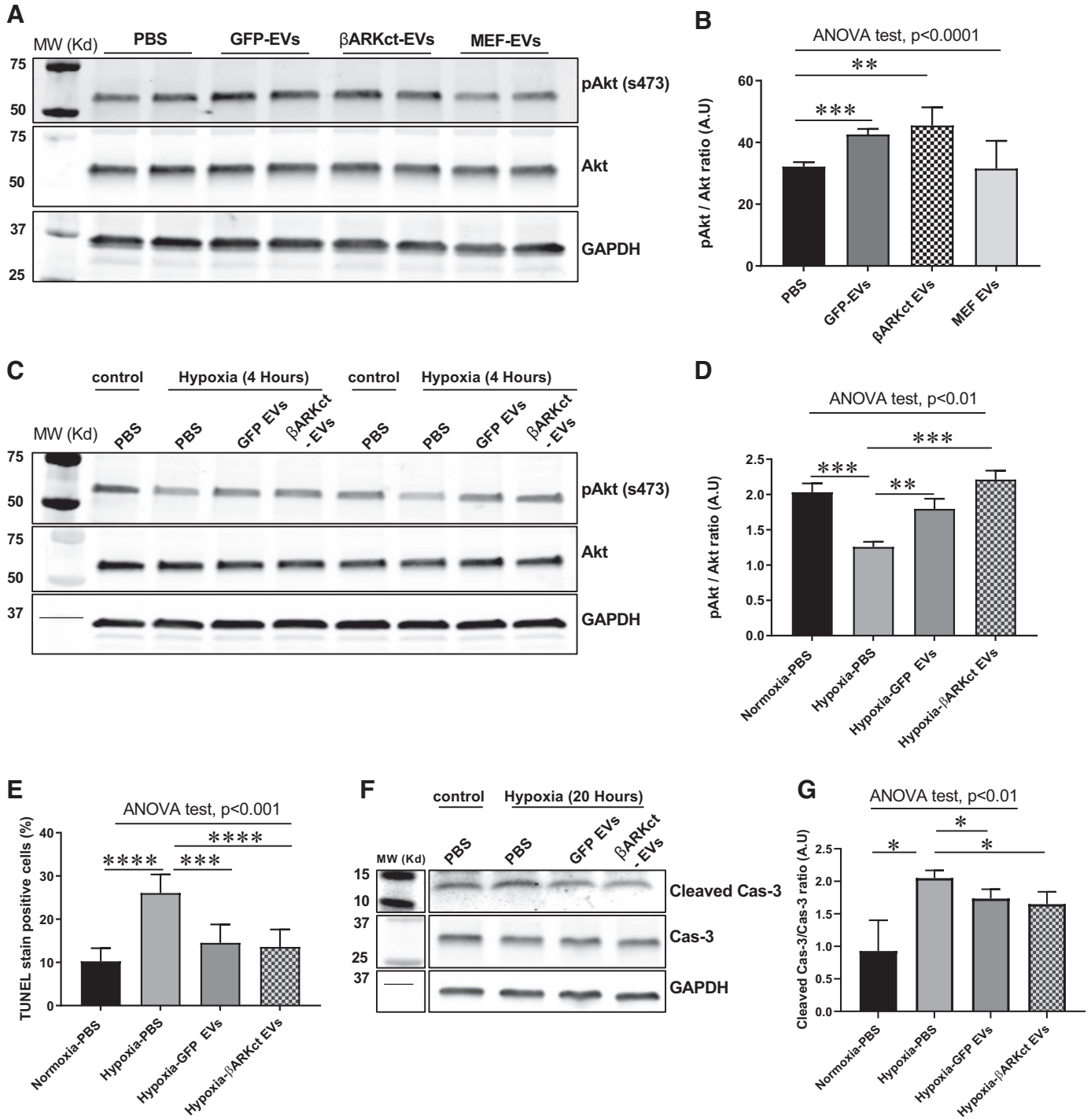

Figure 2. Cardioprotective effect of βARKct and green fluorescent protein (GFP) extracellular vesicles (EVs) in neonatal rat ventricle cardiomyocytes (NRVMs) exposed to hypoxia. *A*: representative immunoblot showing p-Akt level NRVMs treated with extracellular vesicles (EVs). *B*: bar graph of pAkt/Akt ratio. *C*: representative immunoblot of phosphorylation of Akt Ser473 and total Akt after hypoxia treatment in EVs-treated NRVMs. *D*: bar graph of p-Akt/total Akt ratio with hypoxic injury. *E*: bar graph of TUNEL stain positive cells after 20 h hypoxic injury. *F*: representative Western blot of cleaved Cas-3 after 20 h hypoxic injury. *G*: bar graph of cleaved caspase 3/caspase 3 ratio after 20 h hypoxic injury. Means ± SD, ANOVA test *P* value of all results is <0.001 or <0.005 and ANOVA followed by Tukey's multiple comparison test. $^{*}P < 0.05$, $^{**}P < 0.01$, $^{***}P < 0.005$, and $^{****}P < 0.001$ and ANOVA test *P* value of all results is <0.001 or <0.005. In *D*, $n = 4$ different experiments and others $n = 3$ different experiments.

advantage. Therefore, we injected βARKct-CDC EVs and GFP-CDC EVs into the infarcted mouse heart and followed their physiological phenotype for 4 wk. Specifically, 3×10^8 EVs in 15 μL saline were injected into three different areas of the infarcted LV immediately after coronary artery ligation (29). EVs -treated mice were compared to sham-operated controls as well as MI mice injected with saline (PBS) or the same number of EVs from MEFs. We followed these five

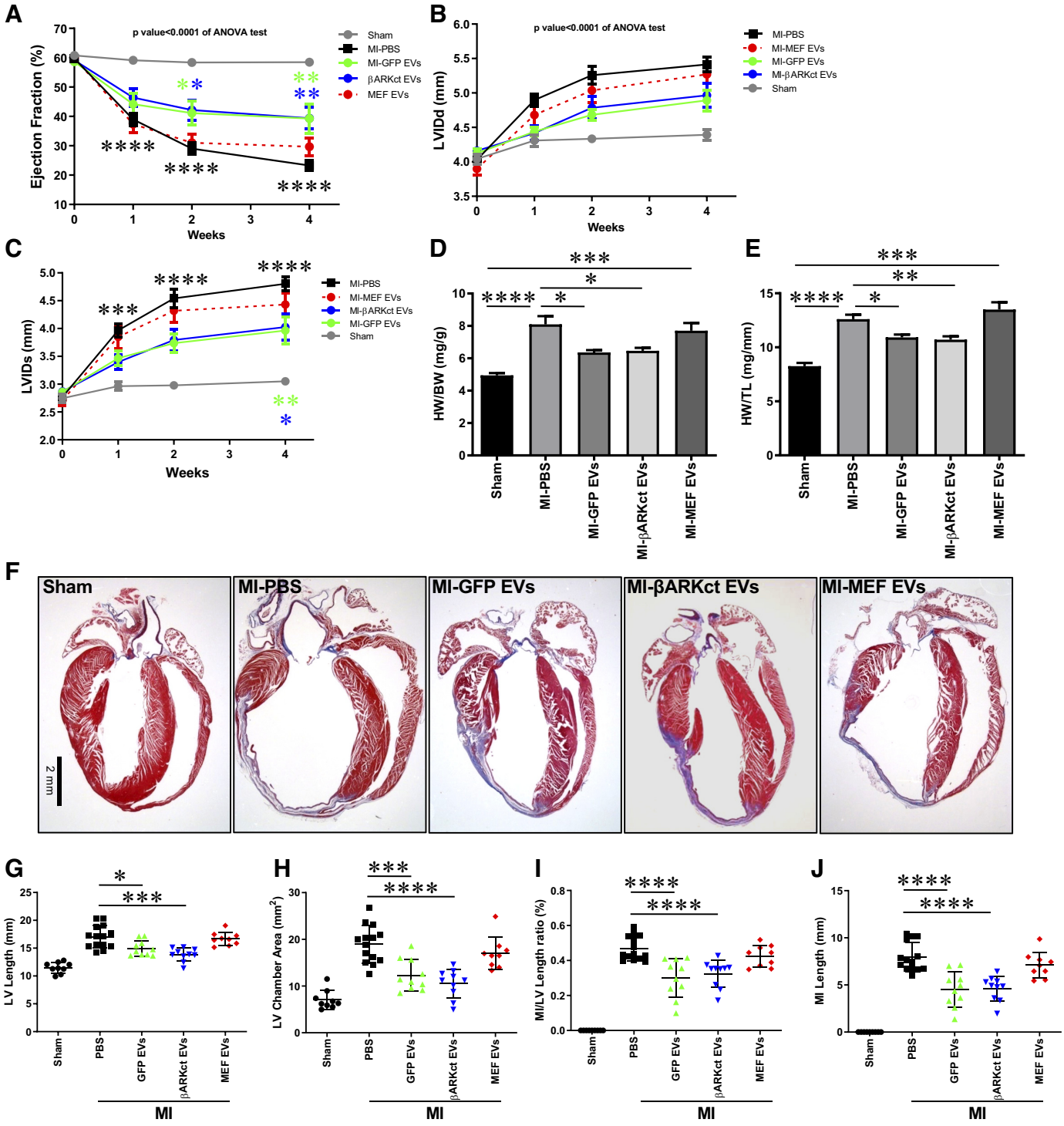

Figure. 3. The green fluorescent protein (GFP) and βARKct extracellular vesicles (EVs) attenuated heart remodeling and preserved heart function after MI. *A–C*: serial measures of cardiac ejection fraction, LVIDd and LVIDs measured at baseline and at 1, 2, and 4 wk post-MI. LV systolic function was preserved by the both cardiac-derived progenitor cell (CDC) extracellular vesicles (EVs) treatment groups compared with MEF EVs and PBS treatments. *D* and *E*: bar graphs of heart weight/body weight ratio and heart weight/tibia length ratio. *F*: representative four chamber view images of Masson Trichrome (MT) staining 4 wk post-MI. *G–J*: bar graphs of histopathological parameters, LV length, LV chamber area, MI/LV length ratio (%), and MI length as measured from tissue sections. Means ± SE, sham ($n = 9$), MI-PBS ($n = 14$), MI-GFP EVs ($n = 10$), MI-βARKct EVs ($n = 11$), MI-MEF EVs ($n = 9$), ANOVA test P value of all results is <0.001 or <0.005 and ANOVA followed by Tukey's multiple comparison test. *$P < 0.05$, **$P < 0.01$, ***$P < 0.005$, and ****$P < 0.001$.

groups of mice by echocardiography (echo) with a pre-MI echo and then at 1, 2, and 4 wk post-MI (Fig. 3, *A–C*). As expected, in the MI mice treated with saline, there was a significant loss of cardiac function as measured by left ventricular (LV) ejection fraction (%EF) at 1 wk post-MI that progressed out to 4 wk ($P < 0.001$ vs. sham) and importantly, injection of EVs from MEFs did not alter the functional response ($P > 0.05$ vs. MI-PBS) (Fig. 3*A*). In contrast, EVs

from both βARKct ($P < 0.05$ vs. MI-PBS) and GFP containing CDCs ($P < 0.01$ vs. MI-PBS) significantly improved cardiac function throughout the 4-wk study period (Fig. 3*A*). Cardiac dilatation is a marker of post-MI heart failure (HF) and LV internal dimensions during systole and diastole were measured as well, and post-MI saline-treated animals showed significant enlargement of the LV by these measures ($P < 0.001$ vs. sham) that was not significantly altered by the MEF-derived EVs ($P > 0.05$ vs. MI-PBS), but both the CDC derived βARKct ($P < 0.05$ vs. MI-PBS) and GFP EVs ($P < 0.01$ vs. MI-PBS) significantly attenuated this pathological enlargement (Fig. 3, *B* and *C*). Since mir-294 has been shown to be an important mediator of beneficial response in myocytes (33), we investigated if this could be why the MEF-EVs did not improve cardiac function, whereas the CDC-derived EVs did. As shown in Supplemental Fig. S2, we found that both types of CDC-EVs contained significantly higher amount of mir-294, indicating the importance of cell-specific cargo miRNA ($P < 0.05$ vs. MEF EVs).

After 4 wk, mice were euthanized and hearts used for morphometric, histological, biochemical, and molecular analyses. As a hallmark of pathological remodeling post-MI, control MI-PBS ($P < 0.001$ vs. sham) and MI-MEF EVs ($P < 0.005$ vs. sham) treated hearts had significantly increased heart weight, normalized to body weight (HW/BW) and tibia length (HW/TL) (Fig. 3, *D* and *E*). Consistent with the echo data above, βARKct-CDC EVs ($P < 0.05$ vs. MI-PBS) and GFP-EVs-treated hearts ($P < 0.05$ vs. MI-PBS) were significantly smaller (Fig. 3, *D* and *E*), which can be visualized in stained sections from the five groups at 4 wk post-MI and treatment (Fig. 3*F*). From these histological sections, several measurements were taken showing that both types of CDC EVs decreased LV remodeling compared with MI-PBS as measured by LV length (GFP EVs; $P < 0.05$ and βARKct EVs; $P < 0.005$) (Fig. 3*G*), LV chamber area (GFP EVs; $P < 0.005$ and βARKct EVs; $P < 0.001$) (Fig. 3*H*), infarct:LV ratio (GFP EVs and βARKct EVs; $P < 0.001$) (Fig. 3*I*), and infarct length (GFP EVs and βARKct EVs; $P < 0.001$) (Fig. 3*J*). Importantly, these significant improvements were not seen in hearts treated with EVs from MEFs, in which LV remodeling and injury did not differ from saline-treated MI hearts ($P > 0.05$) (Fig. 3, *G*–*J*).

Using this MI model, we also addressed whether the EVs had any acute cardioprotective properties and assessed myocardial apoptosis using TUNEL staining of sections 2 days after MI and EVs delivery. We also assessed early inflammatory cell infiltration of the *day 2* post-MI hearts, specifically staining with myeloperoxidase marking neutrophils in the infarcted heart. As shown Fig. 4*A* and *B*, CDC-derived EVs regardless of cargo significantly decreased the apoptotic cardiomyocyte ratio compared with saline (GFP EVs; $P < 0.005$ and βARKct EVs; $P < 0.01$) and MEF-EVs-treated MI hearts (GFP EVs; $P < 0.001$ and βARKct EVs; $P < 0.005$). Furthermore, neutrophils were found significantly up in MI-saline hearts compared with sham ($P < 0.0001$) but CDC EVs treatment regardless of origin had significantly less of these immune cells (GFP EVs; $P < 0.01$ and βARKct EVs; $P < 0.001$) (Fig. 4, *C* and *D*).

We evaluated mRNA levels of key cytokines in heart tissue at the *day 2* post-MI time point and also measured these in the blood via an ELISA. MI increased the mRNA level of proinflammatory cytokines *IL-6* ($P < 0.01$), *MCP-1* ($P < 0.0001$), and *CCL-4* ($P < 0.05$) in the heart compared with sham hearts but not the protective cytokine *IL-10* (Fig. 4*E*). Interestingly, βARKct-CDC EVs had significantly less proinflammatory *IL-6* ($P < 0.05$) and *MCP-1* ($P < 0.05$) compared with any other treatment, demonstrating a clear advantage for these EVs in this model (Fig. 4*E*). GFP-CDC EVs-treated hearts as well as βARKct-CDC EVs-treated hearts both had decreased *BNP* levels showing less remodeling and HF and the βARKct-CDC EVs group trended to be the lowest, consistent with positive results above (GFP EVs; $P < 0.05$ and βARKct EVs; $P < 0.005$ vs. MI-PBS) (Fig. 4*F*).

In blood, first we examined cardiac troponin I (cTnI) as a marker of injury, and as expected, MI mice had significantly elevated levels of this in vivo marker of myocyte death ($P < 0.01$ vs. sham) and all EVs decreased this marker but not significant difference ($P > 0.05$ vs. MI-PBS) (Fig. 4*G*). Furthermore, only GFP-CDC EVs-treated post-MI mice showed a significant decrease of IL-6 ($P < 0.05$ vs. MI-PBS) (Fig. 4*H*), however βARKct-CDC EVs-treated post-MI mice had a significant increase of the anti-inflammatory cytokine IL-10 ($P < 0.01$) (Fig. 4*I*), consistent with βARKct having some beneficial advantage over other EVs, although this did not result in a significant chronic functional benefit.

Effects of β ARKct-CDC EVs versus GFP-CDC EVs in a Catecholamine-Induced Cardiac Injury Model

As a second model of cardiac injury and to gain mechanistic insight, we used a catecholamine toxicity model where high dose isoproterenol (ISO) was delivered to myocytes in vitro. First, in cultured NRVMs, Iso increased the activity of the apoptotic marker caspase 3 in a time-dependent manner, with 16 h ($P < 0.01$ vs. PBS) having higher caspase 3 activation than 4 h ($P < 0.05$ vs. PBS) (Fig. 5, *A* and *B*). Interestingly, GFP-CDC EVs and βARKct-CDC EVs both caused decreased caspase 3 activation following Iso treatment, with βARKct-CDC EVs trending toward better protection in this model, especially at the 16 h time point (GFP EVs; $P > 0.05$ and βARKct EVs $P < 0.05$ vs. Iso) (Fig. 5, *A* and *B*).

In mice, we injected 300 mg/kg/day of Iso dorsal SQ for five consecutive days, which has been shown to cause acute cardiac toxicity that results in significant dysfunction and HF chronically (30). Indeed, we saw significant LV dysfunction via echo at 2 wk post-Iso ($P < 0.001$ vs. PBS) (Fig. 5*C*), and interestingly, βARKct-CDC EVs delivered on *day 1*, before the first Iso injection, totally prevented this dysfunction compared with the control condition of saline ($P < 0.01$) and MEF-EVs treatment ($P < 0.01$), or GFP-CDC EVs ($P < 0.05$) (Fig. 5*C*). This demonstrates that the presence of βARKct in CDC and resulting EVs have differential benefits in this model, and it may have to do with GRK2 inhibition, which is a property of the βARKct peptide (28).

The results in Fig. 5*C* directed us to reexamine in vitro mechanistic effects of βARKct-CDC EVs, and we developed a new injury model for myocytes (NRVMs), which consisted of 20 h of hypoxia combined with 100 μM Iso. The goal of this stress was to mimic high catecholamines after myocardial ischemic injury. We found that myocyte apoptosis was robust ($P < 0.01$ vs. normoxia PBS), and although both types of CDC EVs were effective at reducing cell death (GFP and βARKct

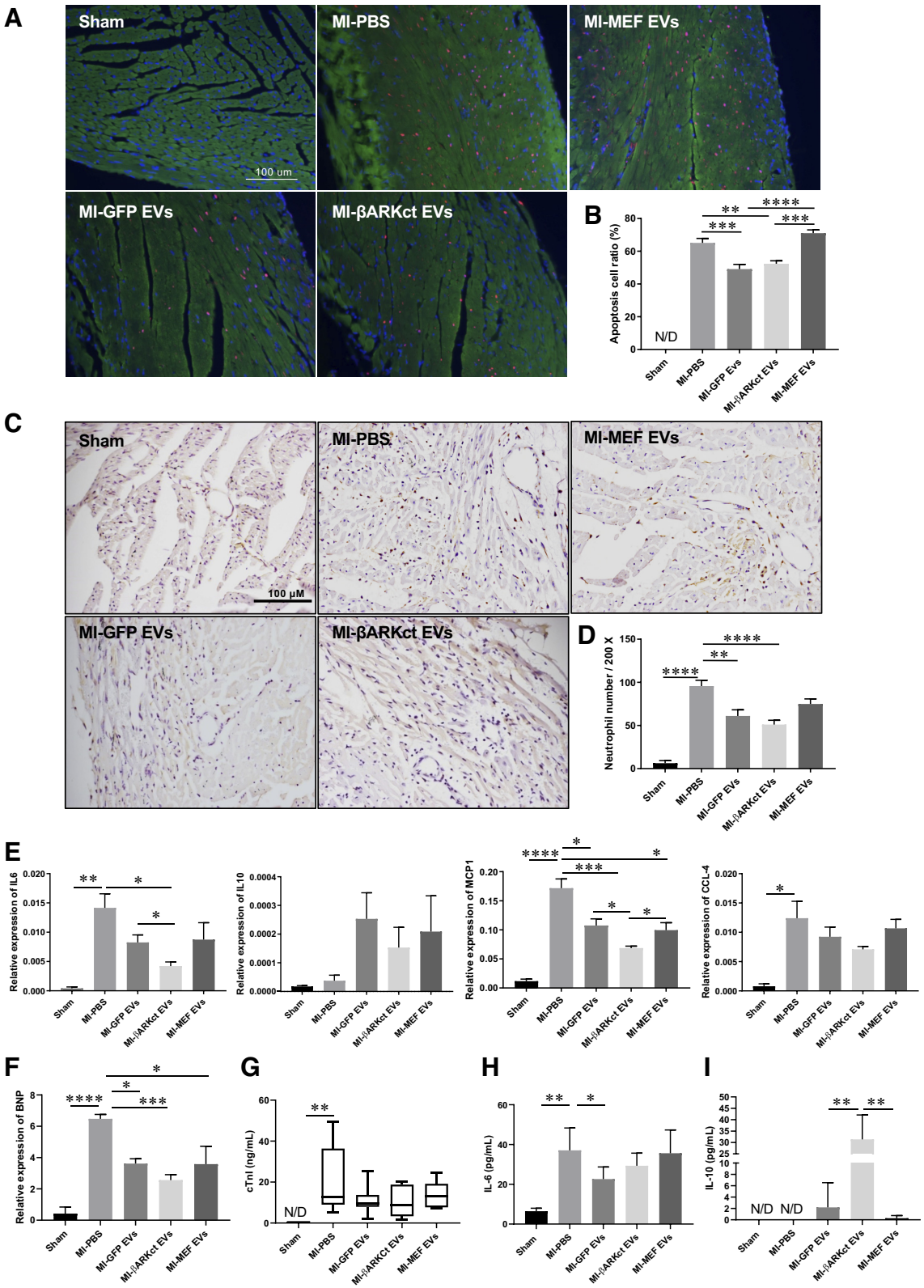

AJP-Heart Circ Physiol • doi:10.1152/ajpheart.00571.2020 • www.ajpheart.org

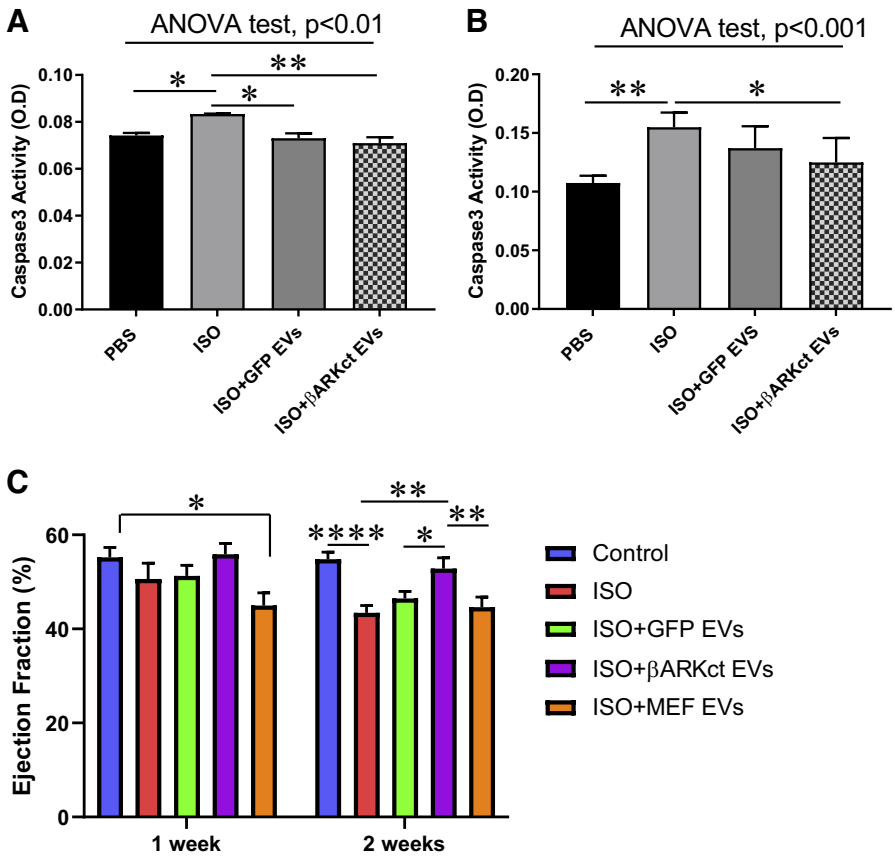

Figure 5. EVs decrease caspase 3 activity in neonatal rat ventricle cardiomyocytes (NRVMs) treated with Iso and improve heart function in vivo. *A* and *B*: activity of caspase 3 measured by colorimetric ELISA at 4 h (*A*) and 16 h (*B*). Means ± SD, $n = 3$. *C*: βARKct EVs improve ejection fraction at 2 wk time point in Iso toxicity model, means ±SE, ANOVA followed by Tukey's multiple comparison test. $^{*}P < 0.05$, $^{**}P < 0.01$, vehicle ($n = 9$), Iso-Veh ($n = 8$), Iso-GFP EVs ($n = 8$), Iso-βARKct EVs ($n = 9$), Iso-MEF EVs ($n = 8$). EVs; extracellular vesicles.

EVs; $P < 0.05$ vs. hypoxia Iso), βARKct-CDC EVs were more beneficial as shown by TUNEL staining ($P < 0.05$ vs. GFP EVs) (Fig. 6*A*). This was also evident in the amount of activated caspase 3 under these conditions (βARKct EVs; $P < 0.05$ vs. Iso) (Fig. 6*B*).

DISCUSSION

After dozens of studies in post-MI models, including clinical trials, using some sort of stem/progenitor cell delivery to regenerate ischemic myocardium, there is consensus that these cells cannot generate new myocytes (34, 35). Even though some studies in animal models showed that cell therapy did improve cardiac structure and function, there was no significant new myocyte formation and the injected cells were usually gone from the heart after several days. There are a few hypotheses for why improvement in post-MI function was found without the continued presence of the cells or appreciable regeneration including the paracrine hypothesis where injected stem cells secrete substances that can improve survival of ischemic myocytes and cause better outcomes (32, 36). A more recent study showed that injection of any cells elicits an inflammatory response in the host myocardium that can lead to changes that stimulate the small improvements seen in cardiac function (37).

In our study, we used secreted EVs from a cardiac-derived progenitor cell that has been shown to improve some small animal models of post-MI remodeling, although they clearly do not regenerate myocytes (17–19, 38), and show that these EVs can improve cardiac function of the post-MI mouse heart when delivered at the time of MI. Furthermore, we tested a CDC line that was engineered to express a known profunction and prosurvival peptide, βARKct, which is an inhibitor of the $G_{\beta\gamma}$-activation of G protein-coupled receptor kinase-2 (GRK2). We have previously reported that when the βARKct is put into these CDCs there is a significant improvement in cell survival, proliferation, metabolism, and β-adrenergic tolerance (22). As GRK2 profoundly affects β-adrenergic receptors in the heart, in addition to the MI model, we used a catecholamine toxicity model to address the effectiveness of

Figure 4. Green fluorescent protein (GFP) and βARKct extracellular vesicles (EVs) injection into LV decreased myocyte cell death and infiltration of inflammatory cell 2 days post-MI. *A*: representative images of TUNEL staining in the myocardium. Green is α-sarcomeric actin, red is TUNEL stain and blue is DAPI. *B*: bar graph of percent TUNEL positive cells. *C*: representative images of neutrophil staining detected by antimyeloperoxidase antibody (MPO, brown color). *D*: bar graph of MPO positive stain cell number. Means ± SE, sham ($n = 5$), MI-PBS ($n = 8$), MI-GFP EVs ($n = 7$), MI-βARKct EVs ($n = 6$), and MI-MEF EVs ($n = 6$). *E*: select cytokine gene level in heart tissue as measured RT-qPCR. *F*: bar graph of BNP mRNA level in heart tissue. *G*: bar graph of cardiac troponin I (cTNI) level in blood. *H* and *I*: quantification of select cytokines in blood. Means ± SE, ANOVA followed by Tukey's multiple comparison test. $^{*}P < 0.05$, $^{**}P < 0.01$, $^{***}P < 0.005$, and $^{****}P < 0.001$. *E*–*I* is sham ($n = 4$), MI-PBS ($n = 4$), MI-GFP EVs ($n = 4$), MI-βARKct EVs ($n = 4$), MI-MEF EVs ($n = 3$), and *G* is $n = 5$–8. *B*, *G*, and *I*, N/D is not detectable. EVs; extracellular vesicles.

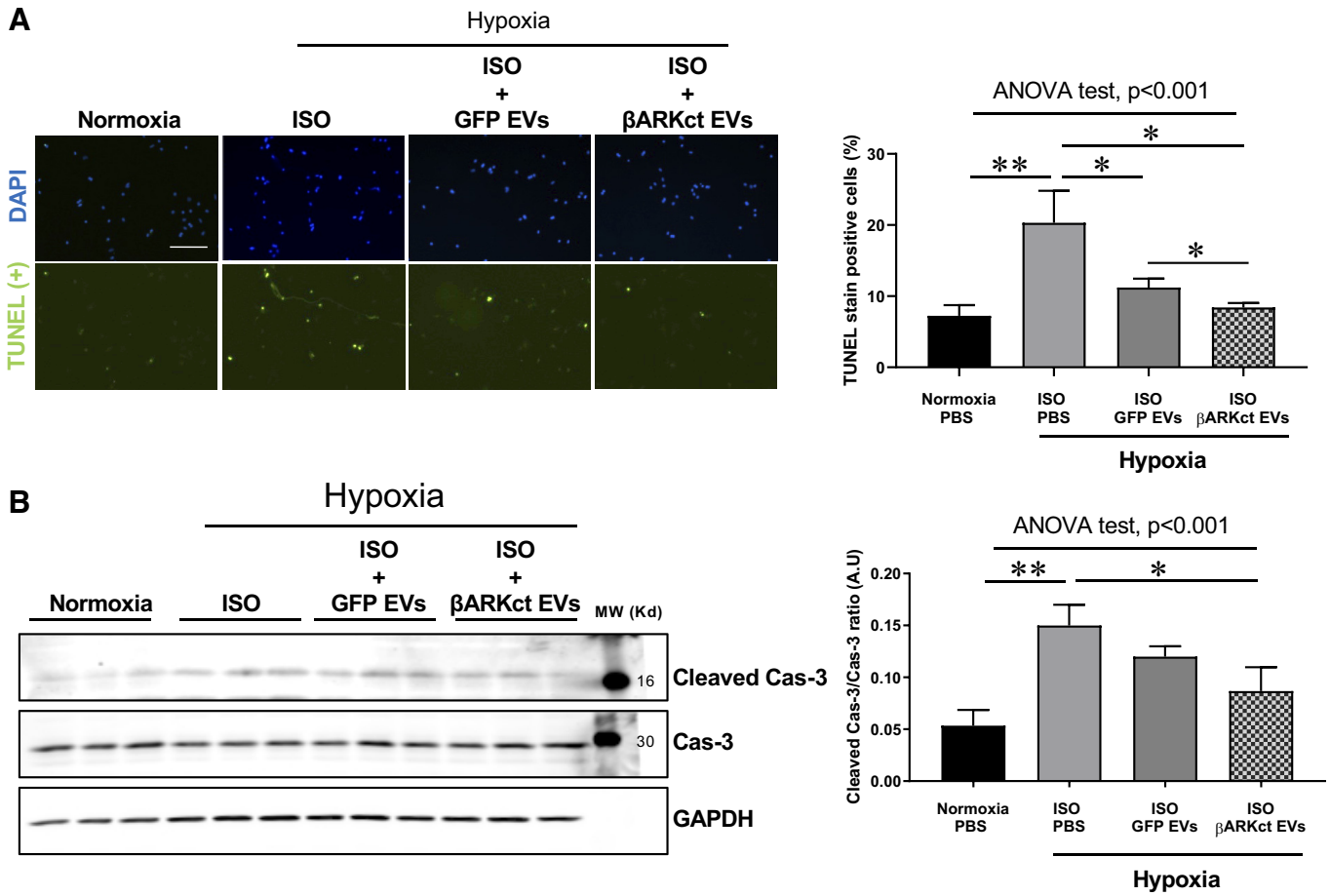

Figure 6. Neonatal rat ventricle cardiomyocytes (NRVMs) treated with βARKct EVs have decreased apoptosis after combined exposure to ISO and hypoxia. *A*: NRVMs were treated with 100 μM Iso then exposed to 20 h of hypoxia. Representative image of TUNEL stain (green) and bar graph showing decreased apoptosis ($n = 3$). White scale bar in *A* is 100 μm. *B*: representative immunoblot and bar graph of normalized cleaved caspase 3 (arbitrary units, AU). Means ± SD, ANOVA followed by Tukey's multiple comparison test or *t* test. $^*P < 0.05$, $^{**}P < 0.01$, $n = 3$. EVs; extracellular vesicles.

these βARKct-CDC EVs and compared them to control CDC EVs purified from cells expressing GFP and also EVs from MEFs. It is important to note that the βARKct-CDC EVs also express GFP via the use of a bicistronic lentivirus to stably engineer these cells with the therapeutic peptide. Importantly, we found that the βARKct was found in the EVs.

Surprisingly, even though the presence of the βARKct improved several cellular phenotypes in the CDCs, EVs from these cells showed minimal differences in micro-RNA cargo compared with GFP-CDC EVs. Previous studies have shown that miRNA cargo is important for any beneficial effects of stem cell exosomes. These studies included beneficial actions of exosomes regulating inhibition of phosphatase and tensin homolog (PTEN) and mTOR signal by exosomal miRNAs such as mir 19a (39) and 21-5p (40). Furthermore, Qiao et al. (40) tested two types of exosomes isolated from explant-derived cardiac stromal cells from patients with HF (FEXO) or from normal donor hearts (NEXO) and compared their regenerative activities in vitro and in vivo. They showed that mir21-5p was upregulated in NEXO exosome whereas FEXO exosomes activated Akt signaling via inhibition of PTEN (40). They also found 13 miRNAs upregulated in NEXO exosomes and, interestingly, we found 7 of the 13 miRNAs in GFP-CDC EVs and 8 of 13 miRNAs in βARKct-CDC EVs within the 20 most highly expressed miRNAs (40). The miR21a-5p was high in both EVs and one such miRNA shown to increase Akt, miR-24-3p, was upregulated in βARKct-CDC. Thus, even though there were minimal changes between our two types of EVs, there were differences that supported our hypothesis that βARKct-containing EVs would be superior in therapeutic efficacy. However, both types of EVs increased Akt activation in myocytes supporting in vitro and in vivo cardioprotection.

Since the βARKct itself was present in these EVs, we posited that they would have more beneficial effects when administered to stressed myocytes in culture or the injured heart in vivo. Thus, we did not expect that even the GFP-CDC EVs would have significant protective effects on myocytes placed in a hypoxic environment. Indeed, both types of CDC EVs improved survival signaling and decreased apoptosis in hypoxic myocytes. This similarity between βARKct-CDC EVs and GFP-CDC EVs extended to beneficial effects in vivo when injected to mouse hearts after permanent LAD occlusion and MI. Importantly, these CDC-derived EVs produced significant improvement in cardiac function up to 4 wk post-MI, and mechanistically, we found less cell death, inflammatory markers, and immune cell infiltration

compared with saline-treated and MEF-EVs-treated controls. One important difference that we did find with βARKct-CDC EVs was improvement in the cytokine profiles with increased anti-inflammatory cytokine IL-10 in the hearts and plasma and lower proinflammatory IL-6. Even though these differential positive effects were seen after βARKct-containing CDC EVs treatments, they did not translate to more beneficial cardiac function, which could mean we missed increased efficacy at shorter or longer windows of observation. Although we focused on apoptosis in this study, necrosis would likely be an important contributor to cell death after MI, as myocytes can die rapidly by necrosis (41). We specifically addressed apoptosis in our mice and cells via TUNEL staining and activated caspase, however we did not directly assess necrosis. This is something that may limit our mechanistic insight; however, it is possible that since ROS can potentiate necrosis, we would see something similar with our CPC-EVs as we did for apoptosis.

Importantly, where we did find an advantage of using βARKct-engineered CDC EVs was in a high catecholamine toxicity and HF model. Compared with control CDC-EVs, βARKct-CDC-EVs prevented LV dysfunction in this model and this could apparently be due to GRK2 inhibition by the transferred βARKct, and improvement in β-adrenergic signaling as we have shown in several other models with βARKct gene therapy in the heart (24–26). Mechanistically, in myocytes exposed to catecholamines as well as hypoxia, βARKct-CDC EVs had superior effects at decreasing cell death, consistent with the improvement in vivo. Future studies can focus on whether EVs are superior in delivering βARKct to the heart over viruses. Furthermore, perhaps incorporating viral vectors carrying the βARKct cDNA into EVs would be advantageous, as some laboratories are promoting (42, 43).

Even though these last experiments did show that βARKct-CDC EVs have some superior properties, in our hands control GFP-CDC EVs also had therapeutic properties, especially evident in the post-MI mouse models. Previous studies using EVs from these cells showed that only EVs from CDCs exposed to 12 h of hypoxia showed cardioprotection in a model of transient ischemia-reperfusion (I/R) injury (18). Mechanistically, this study showed that miRNA cargo in EVs changed when CDCs were exposed to longer periods of hypoxia with miRNAs promoting survival being upregulated (18). The difference in our study that showed normal CDC-EVs increasing cardiac function after MI could be due to the model of permanent coronary artery dilation and larger injury compared with I/R or perhaps our culture conditions support EVs that are more beneficial. Further research is needed to determine these differential effects.

Conclusions

In this report, we showed that βARKct engineering of a cardiac-derived progenitor cell could generate EVs containing this prosurvival and procontractile functional peptide and that these EVs can be delivered to the ischemic and injured heart to provide benefit. Our data would suggest that even though only a few key differences in beneficial effect between CDC-EVs (GFP) and βARKct-CDC EVs were observed, the increase in efficacy in the catecholamine model and the improved cytokine profile in the MI model suggests that this could be something to continue pursuing. Furthermore, EVs from these cells, at least in mouse models, provide robust therapeutic efficacy. Perhaps, combining βARKct EVs with other types of EVs with known angiogenic effects, for example, would be advantageous to elicit prosurvival signaling and increase perfusion of the injured myocardium.

ACKNOWLEDGMENTS

We thank Zuping Qu for mouse husbandry and Dr. Efimov from the Bio Imaging Facility at Fox Chase Cancer Center for the EM sample preparation and imaging.

Present address of S. M. Schumacher: Cardiovascular & Metabolic Sciences, Lerner Research Inst., Cleveland Clinic, Cleveland, OH.

GRANTS

This work was supported by National Institutes of Health (NIH) Grants P01 HL134608 (to W.J.K.), P01 HL075443 (to W.J.K.), R01 HL061690 (to W.J.K.), and an award from the American Heart Association (AHA) 18MERIT33900036 (to W.J.K.).

DISCLOSURES

No conflicts of interest, financial or otherwise, are declared by the authors.

AUTHOR CONTRIBUTIONS

J.-S.K., R.K., and W.J.K. conceived and designed research; J.-S.K., S.M.S., E.G., J.I., and R.R performed experiments; J.-S.K. and S.M.S. analyzed data; J.-S.K. and W.J.K. interpreted results of experiments; J.-S.K. prepared figures; J.-S.K. and W.J.K. drafted manuscript; J.-S.K., J.K.C., R.K., and W.J.K. edited and revised manuscript; J-S.K., S.M.S., E.G., J.K.C., J.I., R.R., M.K., R.K., and W.J.K. approved final version of manuscript.

REFERENCES

1. **Ward MR**, **Abadeh A**, **Connelly KA.** Concise review: rational use of mesenchymal stem cells in the treatment of ischemic heart disease. *Stem Cells Transl Med* 7: 543–550, 2018. doi:10.1002/sctm.17-0210.
2. **Gallet R**, **Dawkins J**, **Valle J**, **Simsolo E**, **de Couto G**, **Middleton R**, **Tseliou E**, **Luthringer D**, **Kreke M**, **Smith RR**, **Marban L**, **Ghaleb B**, **Marban E.** Exosomes secreted by cardiosphere-derived cells reduce scarring, attenuate adverse remodelling, and improve function in acute and chronic porcine myocardial infarction. *Eur Heart J* 38: 201–211, 2017. doi:10.1093/eurheartj/ehw240.
3. **Gallina C**, **Turinetto V**, **Giachino C.** A new paradigm in cardiac regeneration: the mesenchymal stem cell secretome. *Stem Cells Int* 2015: 765846, 2015. doi:10.1155/2015/765846.
4. **Trac D**, **Hoffman JR**, **Bheri S**, **Maxwell JT**, **Platt MO**, **Davis ME.** Predicting functional responses of progenitor cell exosome potential with computational modeling. *Stem Cells Transl Med* 8: 1212–1221, 2019. doi:10.1002/sctm.19-0059.
5. **Gnecchi M**, **He H**, **Liang OD**, **Melo LG**, **Morello F**, **Mu H**, **Noiseux N**, **Zhang L**, **Pratt RE**, **Ingwall JS**, **Dzau VJ.** Paracrine action accounts for marked protection of ischemic heart by Akt-modified mesenchymal stem cells. *Nat Med* 11: 367–368, 2005. doi:10.1038/nm0405-367.
6. **Zernecke A**, **Bidzhekov K**, **Noels H**, **Shagdarsuren E**, **Gan L**, **Denecke B**, **Hristov M**, **Koppel T**, **Jahantigh MN**, **Lutgens E**, **Wang S**, **Olson EN**, **Schober A**, **Weber C.** Delivery of microRNA-126 by apoptotic bodies induces CXCL12-dependent vascular protection. *Sci Signal* 2: ra81, 2009. doi:10.1126/scisignal.2000610.

7. **Yang VK**, **Loughran KA**, **Meola DM**, **Juhr CM**, **Thane KE**, **Davis AM**, **Hoffman AM.** Circulating exosome microRNA associated with heart failure secondary to myxomatous mitral valve disease in a naturally occurring canine model. *J Extracell Vesicles* 6: 1350088, 2017. doi:10.1080/20013078.2017.1350088.
8. **Patil M**, **Henderson J**, **Luong H**, **Annamalai D**, **Sreejit G**, **Krishnamurthy P.** The art of intercellular wireless communications: exosomes in heart disease and therapy. *Front Cell Dev Biol* 7: 315, 2019. doi:10.3389/fcell.2019.00315.
9. **Witwer KW**, **Buzas EI**, **Bemis LT**, **Bora A**, **Lasser C**, **Lotvall J**, **Nolte-'t Hoen EN**, **Piper MG**, **Sivaraman S**, **Skog J**, **Thery C**, **Wauben MH**, **Hochberg F.** Standardization of sample collection, isolation and analysis methods in extracellular vesicle research. *J Extracell Vesicles* 2: 10, 2013. doi:10.3402/jev.v2i0.20360.
10. **Raposo G**, **Stoorvogel W.** Extracellular vesicles: exosomes, microvesicles, and friends. *J Cell Biol* 200: 373–383, 2013. doi:10.1083/jcb.201211138.
11. **Xu R**, **Greening DW**, **Zhu H-J**, **Takahashi N**, **Simpson RJ.** Extracellular vesicle isolation and characterization: toward clinical application. *J Clin Invest* 126: 1152–1162, 2016. doi:10.1172/JCI81129.
12. **Das S**, **Halushka MK.** Extracellular vesicle microRNA transfer in cardiovascular disease. *Cardiovasc Pathol* 24: 199–206, 2015. doi:10.1016/j.carpath.2015.04.007.
13. **Kalluri R.** The biology and function of exosomes in cancer. *J Clin Invest* 126: 1208–1215, 2016. doi:10.1172/JCI81135.
14. **Andre F**, **Chaput N**, **Schartz NEC**, **Flament C**, **Aubert N**, **Bernard J**, **Lemonnier F**, **Raposo G**, **Escudier B**, **Hsu D-H**, **Tursz T**, **Amigorena S**, **Angevin E**, **Zitvogel L.** Exosomes as potent cell-free peptide-based vaccine. I. Dendritic cell-derived exosomes transfer functional MHC class I/peptide complexes to dendritic cells. *J Immunol* 172: 2126–2136, 2004. doi:10.4049/jimmunol.172.4.2126.
15. **Hartman ZC**, **Wei J**, **Glass OK**, **Guo H**, **Lei G**, **Yang X-Y**, **Osada T**, **Hobeika A**, **Delcayre A**, **Le Pecq J-B**, **Morse MA**, **Clay TM**, **Lyerly HK.** Increasing vaccine potency through exosome antigen targeting. *Vaccine* 29: 9361–9367, 2011. doi:10.1016/j.vaccine.2011.09.133.
16. **Besse B**, **Charrier M**, **Lapierre V**, **Dansin E**, **Lantz O**, **Planchard D**, **Le Chevalier T**, **Livartoski A**, **Barlesi F**, **Laplanche A**, **Ploix S**, **Vimond N**, **Peguillet I**, **Thery C**, **Lacroix L**, **Zoernig I**, **Dhodapkar K**, **Dhodapkar M**, **Viaud S**, **Soria J-C**, **Reiners KS**, **von Strandmann EP**, **Vely F**, **Rusakiewicz S**, **Eggermont A**, **Pitt JM**, **Zitvogel L**, **Chaput N.** Dendritic cell-derived exosomes as maintenance immunotherapy after first line chemotherapy in NSCLC. *Oncoimmunology* 5: e1071008, 2016. doi:10.1080/2162402X.2015.1071008.
17. **Chen L**, **Wang Y**, **Pan Y**, **Zhang L**, **Shen C**, **Qin G**, **Ashraf M**, **Weintraub N**, **Ma G**, **Tang Y.** Cardiac progenitor-derived exosomes protect ischemic myocardium from acute ischemia/reperfusion injury. *Biochem Bioph Res Commun* 431: 566–571, 2013. doi:10.1016/j.bbrc.2013.01.015.
18. **Gray WD**, **French KM**, **Ghosh-Choudhary S**, **Maxwell JT**, **Brown ME**, **Platt MO**, **Searles CD**, **Davis ME.** Identification of therapeutic covariant microRNA clusters in hypoxia-treated cardiac progenitor cell exosomes using systems biology. *Circ Res* 116: 255–263, 2015. doi:10.1161/CIRCRESAHA.116.304360.
19. **Vrijsen KR**, **Sluijter JPG**, **Schuchardt MWL**, **van Balkom BWM**, **Noort WA**, **Chamuleau SAJ**, **Doevendans PAFM.** Cardiomyocyte progenitor cell-derived exosomes stimulate migration of endothelial cells. *J Cell Mol Med* 14: 1064–1070, 2010. doi:10.1111/j.1582-4934.2010.01081.x.
20. **van Berlo JH**, **Kanisicak O**, **Maillet M**, **Vagnozzi RJ**, **Karch J**, **Lin S-CJ**, **Middleton RC**, **Marban E**, **Molkentin JD.** c-kit$^+$ cells minimally contribute cardiomyocytes to the heart. *Nature* 509: 337–341, 2014. doi:10.1038/nature13309.
21. **Molkentin JD**, **Houser SR.** Are resident c-Kit$^+$ cardiac stem cells really all that are needed to mend a broken heart? *Circ Res* 113: 1037–1039, 2013. doi:10.1161/CIRCRESAHA.113.302564.
22. **Khan M**, **Mohsin S**, **Toko H**, **Alkatib M**, **Nguyen J**, **Truffa S**, **Gude N**, **Chuprun K**, **Tilley DG**, **Koch WJ**, **Sussman MA.** Cardiac progenitor cells engineered with βARKct have enhanced β-adrenergic tolerance. *Mol Ther* 22: 178–185, 2014. doi:10.1038/mt.2013.200.
23. **Sato PY**, **Chuprun JK**, **Schwartz M**, **Koch WJ.** The evolving impact of g protein-coupled receptor kinases in cardiac health and disease. *Physiol Rev* 95: 377–404, 2015. doi:10.1152/physrev.00015.2014.
24. **Raake PWJ**, **Schlegel P**, **Ksienzyk J**, **Reinkober J**, **Barthelmes J**, **Schinkel S**, **Pleger S**, **Mier W**, **Haberkorn U**, **Koch WJ**, **Katus HA**, **Most P**, **Muller OJ.** AAV6.βARKct cardiac gene therapy ameliorates cardiac function and normalizes the catecholaminergic axis in a clinically relevant large animal heart failure model. *Eur Heart J* 34: 1437–1447, 2013. doi:10.1093/eurheartj/ehr447.
25. **Rengo G**, **Lymperopoulos A**, **Zincarelli C**, **Donniacuo M**, **Soltys S**, **Rabinowitz JE**, **Koch WJ.** Myocardial adeno-associated virus serotype 6-betaARKct gene therapy improves cardiac function and normalizes the neurohormonal axis in chronic heart failure. *Circulation* 119: 89–98, 2009. doi:10.1161/CIRCULATIONAHA.108.803999.
26. **Shah AS**, **White DC**, **Emani S**, **Kypson AP**, **Lilly RE**, **Wilson K**, **Glower DD**, **Lefkowitz RJ**, **Koch WJ.** In vivo ventricular gene delivery of a beta-adrenergic receptor kinase inhibitor to the failing heart reverses cardiac dysfunction. *Circulation* 103: 1311–1316, 2001. doi:10.1161/01.cir.103.9.1311.
27. **Filipe V**, **Hawe A**, **Jiskoot W.** Critical evaluation of Nanoparticle Tracking Analysis (NTA) by NanoSight for the measurement of nanoparticles and protein aggregates. *Pharm Res* 27: 796–810, 2010. doi:10.1007/s11095-010-0073-2.
28. **Brinks H**, **Boucher M**, **Gao E**, **Chuprun JK**, **Pesant S**, **Raake PW**, **Huang ZM**, **Wang X**, **Qiu G**, **Gumpert A**, **Harris DM**, **Eckhart AD**, **Most P**, **Koch WJ.** Level of G protein-coupled receptor kinase-2 determines myocardial ischemia/reperfusion injury via pro- and anti-apoptotic mechanisms. *Circ Res* 107: 1140–1149, 2010. doi:10.1161/CIRCRESAHA.110.221010.
29. **Gao E**, **Lei YH**, **Shang X**, **Huang ZM**, **Zuo L**, **Boucher M**, **Fan Q**, **Chuprun JK**, **Ma XL**, **Koch WJ.** A novel and efficient model of coronary artery ligation and myocardial infarction in the mouse. *Circ Res* 107: 1445–1453, 2010. doi:10.1161/CIRCRESAHA.110.223925.
30. **Wallner M**, **Duran JM**, **Mohsin S**, **Troupes CD**, **Vanhoutte D**, **Borghetti G**, **Vagnozzi R**, **Gross P**, **Yu D**, **Trappanese DM**, **Kubo H**, **Toib A**, **Sharp TE 3rd**, **Harper SC**, **Volkert MA**, **Starosta T**, **Feldsott EA**, **Berretta RM**, **Wang T**, **Barbe MF**, **Molkentin JD**, **Houser SR.** Acute catecholamine exposure causes reversible myocyte injury without cardiac regeneration. *Circ Res* 119: 865–879, 2016. doi:10.1161/CIRCRESAHA.116.308687.
31. **Schumacher SM**, **Gao E**, **Cohen M**, **Lieu M**, **Chuprun JK**, **Koch WJ.** A peptide of the RGS domain of GRK2 binds and inhibits Gα(q) to suppress pathological cardiac hypertrophy and dysfunction. *Sci Signal* 9: ra30, 2016. doi:10.1126/scisignal.aae0549.
32. **Marban E.** The secret life of exosomes: what bees can teach us about next-generation therapeutics. *J Am Coll Cardiol* 71: 193–200, 2018. doi:10.1016/j.jacc.2017.11.013.
33. **Khan M**, **Nickoloff E**, **Abramova T**, **Johnson J**, **Verma SK**, **Krishnamurthy P**, **Mackie AR**, **Vaughan E**, **Garikipati VNS**, **Benedict C**, **Ramirez V**, **Lambers E**, **Ito A**, **Gao E**, **Misener S**, **Luongo T**, **Elrod J**, **Qin G**, **Houser SR**, **Koch WJ**, **Kishore R.** Embryonic stem cell-derived exosomes promote endogenous repair mechanisms and enhance cardiac function following myocardial infarction. *Circ Res* 117: 52–64, 2015. doi:10.1161/CIRCRESAHA.117.305990.
34. **Cai C-L**, **Molkentin JD.** The elusive progenitor cell in cardiac regeneration: slip slidin' away. *Circ Res* 120: 400–406, 2017. doi:10.1161/CIRCRESAHA.116.309710.
35. **Gyongyosi M**, **Haller PM**, **Blake DJ**, **Martin Rendon E.** Meta-analysis of cell therapy studies in heart failure and acute myocardial infarction. *Circ Res* 123: 301–308, 2018. doi:10.1161/CIRCRESAHA.117.311302.
36. **Kishore R**, **Khan M.** More than tiny sacks: stem cell exosomes as cell-free modality for cardiac repair. *Circ Res* 118: 330–343, 2016. doi:10.1161/CIRCRESAHA.115.307654.
37. **Vagnozzi RJ**, **Maillet M**, **Sargent MA**, **Khalil H**, **Johansen AKZ**, **Schwanekamp JA**, **York AJ**, **Huang V**, **Nahrendorf M**, **Sadayappan S**, **Molkentin JD.** An acute immune response underlies the benefit of cardiac stem cell therapy. *Nature* 577: 405–409, 2020. doi:10.1038/s41586-019-1802-2.
38. **Youn S-W**, **Li Y**, **Kim Y-M**, **Sudhahar V**, **Abdelsaid K**, **Kim HW**, **Liu Y**, **Fulton DJR**, **Ashraf M**, **Tang YL**, **Fukai T**, **Ushio-Fukai M.** Modification of cardiac progenitor cell-derived exosomes by miR-322 provides protection against myocardial infarction through Nox2-dependent angiogenesis. *Antioxidants (Basel)* 8: 18, 2019. doi:10.3390/antiox8010018.
39. **Yu B**, **Kim HW**, **Gong M**, **Wang J**, **Millard RW**, **Wang Y**, **Ashraf M**, **Xu M.** Exosomes secreted from GATA-4 overexpressing mesenchymal stem cells serve as a reservoir of anti-apoptotic microRNAs for

cardioprotection. *Int J Cardiol* 182: 349–360, 2015. doi:10.1016/j.ijcard.2014.12.043.

40. **Qiao L**, **Hu S**, **Liu S**, **Zhang H**, **Ma H**, **Huang K**, **Li Z**, **Su T**, **Vandergriff A**, **Tang J**, **Allen T**, **Dinh P-U**, **Cores J**, **Yin Q**, **Li Y**, **Cheng K.** microRNA-21-5p dysregulation in exosomes derived from heart failure patients impairs regenerative potential. *J Clin Invest* 129: 2237–2250, 2019. doi:10.1172/JCI123135.
41. **Elrod JW**, **Wong R**, **Mishra S**, **Vagnozzi RJ**, **Sakthievel B**, **Goonasekera SA**, **Karch J**, **Gabel S**, **Farber J**, **Force T**, **Brown JH**, **Murphy E**, **Molkentin JD.** Cyclophilin D controls mitochondrial pore–dependent Ca^{2+} exchange, metabolic flexibility, and propensity for heart failure in mice. *J Clin Invest* 120: 3680–3687, 2010. doi:10.1172/JCI43171.
42. **Adamiak M**, **Sahoo S.** Exosomes in myocardial repair: advances and challenges in the development of next-generation therapeutics. *Mol Ther* 26: 1635–1643, 2018. doi:10.1016/j.ymthe.2018.04.024.
43. **Wassmer SJ**, **Carvalho LS**, **György B**, **Vandenberghe LH**, **Maguire CA.** Exosome-associated AAV2 vector mediates robust gene delivery into the murine retina upon intravitreal injection. *Sci Rep* 7: 45329, 2017. doi:10.1038/srep45329.